Damping Pressure Pulsations in a Wave-Powered Desalination System

Brandon J. Hopkins, Nikhil Padhye [*]**, Alison Greenlee,**
James Torres, Levon Thomas, Dean M. Ljubicic, Mortiz P. Kassner
Alexander H. Slocum
Department of Mechanical Engineering
MIT, Cambridge, MA 02139

Email: npdhye,slocum@mit.edu

ABSTRACT

Wave-driven reverse osmosis desalination systems can be a cost-effective option for providing a safe and reliable source of drinking water for large coastal communities. Such systems usually require the stabilization of pulsating pressures for desalination purposes. The key challenge is to convert a fluctuating pressure flow into a constant pressure flow. To address this task, stub-filters, accumulators, and radially elastic-pipes are considered for smoothing the pressure fluctuations in the flow. An analytical model for fluidic capacitance of accumulators and elastic pipes are derived and verified. Commercially available accumulators in combination with essentially rigid (and low cost) piping are found to be a cost-effective solution for this application, and a model for selecting accumulators with the required fluidic-capacitance for the intended system is thus presented.

1 Introduction

Approximately 38% of 1.1 billion people lacking access to safe drinking water reside in coastal areas [1] where access to wave energy is abundant. Fossil fuels are used to produce potable water in existing desalination processes, but the availability of fossil fuels is limited [2, 3]. Thus, using renewables to drive desalination processes and to provide energy to coastal areas is gaining popularity [4–9].

An ongoing project at Resolute Marine Energy (RME), outlined in Figure 1, uses ocean waves to power a desalination machine that filters beach-well water to provide potable water. The advancing and receding waves drive a wave-paddle pump that pushes beach-well water through a reverse-osmosis (RO) membrane. The cyclical nature of the waves causes the pump to push the beach-well water in pulses. In order to achieve successful filtration, however, the incoming beach-well water must be delivered to the RO membrane at a relatively constant pressure, 6.2 ± 0.3 MPa. For the application at hand, the RO system uses an energy recovery unit that allows water to be fed into the RO system at 3.5 ± 0.1 MPa. The pressure fluctuations generated by the wave-paddle pump can be modeled as a sinusoid with a period of 5 seconds and a peak to trough pressure variation of 6.9 to 0 MPa. The desire flow rate of the whole system is approximately 174 l/min. The purpose of this paper is to identify a low-cost, robust, energy-efficient solution that rapidly damps the pressure pulsations generated by the wave-paddle, 6.9 to 0 MPa, to an acceptable constant feed pressure, 3.5 ± 0.1 MPa, to the RO system.

The paper is outlined as follows. Novel and commonly used methods to smooth pressure are outlined in section 2. Stub filters that use destructive interference to smooth pressure are analyzed and found to be inappropriate for the given application. Off-the-shelf accumulators that use fluidic capacitance to damp pressure pulsations are investigated. Elastic pipes are also studied as a potential pressure-smoothing alternative. Several shapes of elastic pipes are studied in section 3 to identify which shape of pipe can produce the largest amount of fluidic capacitance for the lowest cost. Based on this investigation, a novel spherical-node design is also proposed. In section 4, a lumped-element model is created describing the entire wave-paddle-RO system to estimate how much fluidic capacitance is needed for the given application. The model

---

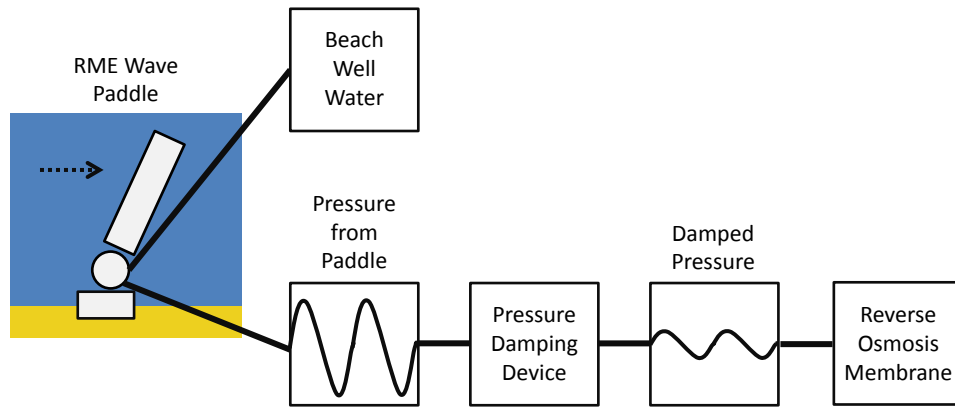[*]Address all correspondence for any issues to this author.

Fig. 1. Schematic of Resolute Marine Energy [10] wave-powered desalination system. The paddle, driven by ocean waves, powers a pump that sucks water from a beach well and pushes it towards a reverse osmosis membrane. The pressure pulsations in the beach well water are stablized by a pressure damping device.

is experimentally investigated in section 5. The cost of the spherical-node design and off-the-shelf accumulators with the necessary fluidic capacitance are calculated in section 6, and off-the-shelf accumulators are found to be the most economical solution. The conclusions are summarized in section 7.

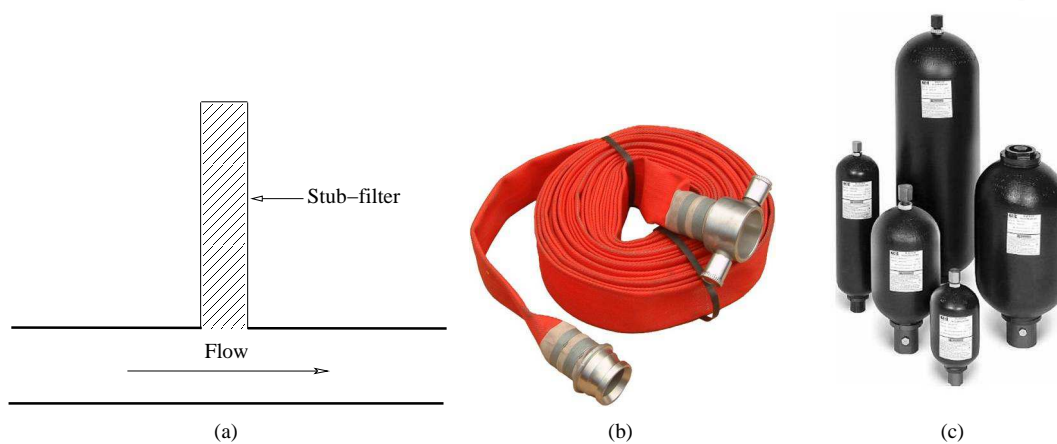## 2   Pressure Smoothing Methods

Fig. 2.   (a) Stub-filters (b) Elastic Pipe and (c) Accumulators.

A stub filter, shown in Figure 2(a), is a long straight pipe attached orthogonally to the flow direction of a pipe. Pressure waves travel up the orthogonal pipe, reflect off the end of the pipe, return to the central pipe, and cancel out pressure waves of a specific frequency. For a given frequency $\omega\ rad/sec$ and a wave-speed $a\ m/s$ which in this case is the speed of sound in water, an appropriate pipe-length $l\ m$ of a stub filter can be calculated as follows [11].

$$l = \frac{\pi}{4}\frac{a}{\omega} \tag{1}$$

If pressure waves travel at approximately $1000\ m/s$ at a frequency of about $0.2\ Hz$, the length of the pipe needed would be more than $500\ m$, which is impractical. Other filters that utilize the same principle of destructive-wave interference, such as H filters, also exist but they fail to attenuate the pressure over a large frequency ranges [11]. Due to these limitations, stub filters are not considered.

An accumulator, Figure 2(c), is a device that is connected to a fluid line and has a mechanism that expands or contracts according to pressure fluctuations in the fluid line. The expansion and contraction of the device smoothes pressure
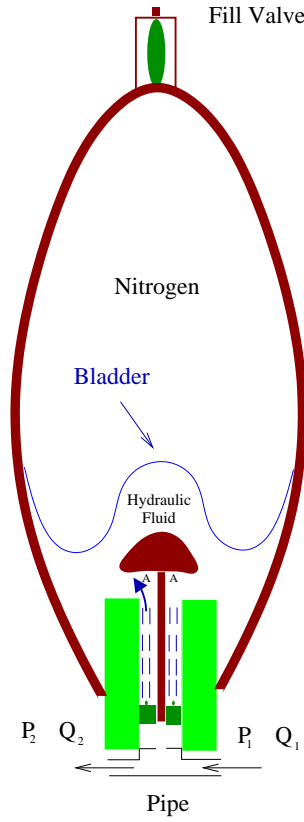
Fig. 3. Bladder accumulator.

fluctuations. There are a variety of accumulators available for a wide range of applications. This study will focus on bladder accumulators as they have a large acceptable pressure fluctuation range and rapidly react to pressure pulsation. Figure 3 shows the inner workings of a bladder accumulator. A bladder usually filled with nitrogen gas is encased in an outer metal exterior shell. The nitrogen is initially pressurized to a specific pressure or precharge pressure. If the pressure in the flow line increases, the bladder contracts and liquid from the line flows into the accumulator. If the pressure in the line decreases, the bladder expands and liquid in the accumulator flows out back to the line. Fluidic capacitance is the fluidic analogue of capacitance in an electrical circuit. Just like electrical capacitors, fluidic capacitors store and release energy into a system. In a fluid system, the capacitance is defined as follows.

$$C_f = \frac{\triangle V}{\triangle P} \tag{2}$$

In equation 2, $\triangle V$ and $\triangle P$ are increments in the volume and the internal pressure respectively. According to the above definition, the fluidic capacitance of a bladder accumulator is given as follows [12].

$$C_{accumulator} = \frac{P_{charged} V_{accumulator}}{P_{line}^2} \tag{3}$$

In equation 3, $P_{charged}$ is the pre-charge pressure of the filled gas, $V_{accumlator}$ is the volume of the accumulator and P_{line} is the line pressure. The greater the available fluidic capacitance, the more the pressure fluctuations in a line will be smoothed.

Accumulators have been used for decades to smooth pressure fluctuations in pipelines, but the pipes themselves can expand and contract just as the bladder in the accumulator to smooth pressure fluctuations. If the pipeline connecting the wave paddle to the RO system is made of a compliant material, the pipeline itself can be designed so that fluidic capacitance is inherently in the pipe itself without the use of an accumulator. Also bladder accumulators must be maintained regularly because the bladders fatigue and rupture regularly. If the capacitance was built into the pipe itself and the pressure fluctuations induced stresses below the yield of the material, perhaps a maintenance-free low cost solution could be designed. Using 2, the fluidic capacitance of various pipes can be calculated.
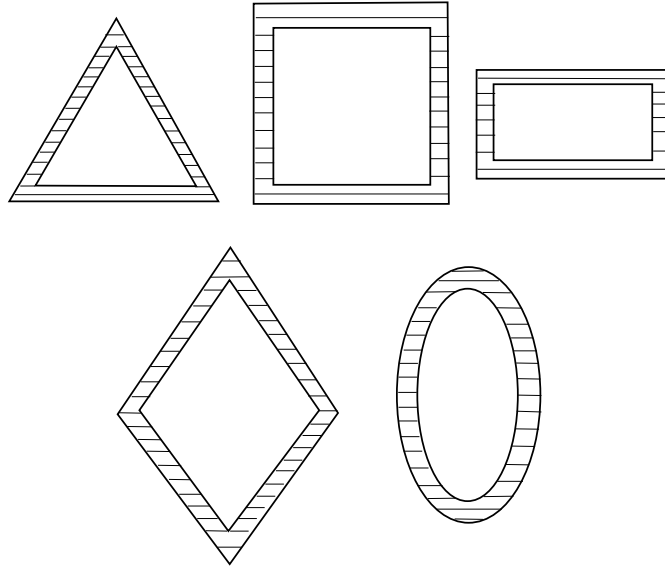
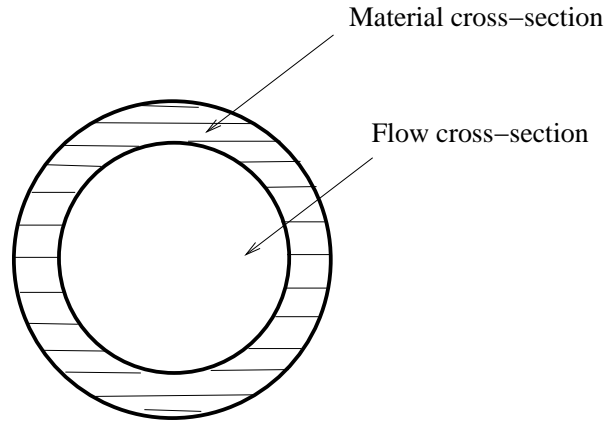Fig. 4.   Different shapes tested for pipe.

Fig. 5.   Material and flow cross-sections in the pipe.

3   Analysis of Elastic Piping

Since we are not limited to the choice of a circular cross-sectional pipe, it is worth exploring whether pipes with different cross-sections can lead to enhanced fluidic capacitance. It is assumed that the pipes are free to expand and contract and that gravity effects are negligible. In the case of a circular cross-section pipe the volume of material per unit capacitance is defined as follows and is derived in the Appendix.

$$m_{pipe} = \frac{4PE}{\sigma_y{}^2} \tag{4}$$

In equation 4, P is the pressure variation, E is the elastic modulus, and σ_y is the yield stress.

Circular, triangular, square, rectangular, rhombic, and elliptical cross-sectional pipes are studied. Analytical models are constructed for circular and triangular cross-sections and compared with respective finite element models. Other cross-sections are modeled using the finite element. Different pipes are defined to have the same internal pressure, maximum von Mises stress, and fluidic capacitance. In the Appendix, it is shown that the pressure drop across the pipe is small relative to the absolute pressure in the pipe. By fixing these parameters, the flow cross-section and material cross-section are determined for each pipe shape.

Table 1 demonstrates that the circular cross-section requires 4 to 5 times less material than the amount of material required for the triangular cross-section to achieve the same fluidic capacitance. The stress concentrations at the corners of the triangle require extra wall-thickness to limit the maximum von Mises stress and thereby require a large material cross-section as can be seen in Figure 6. Also, the flow area for the circular pipe is larger than the flow area for the triangular pipe.

Table 1. Comparison between FEA and analytical results.

Input: Independent Parameters				
	Circular Pipe		Triangular Pipe	
	FEA	Analytical	FEA	Analytical
Pressure (*MPa*)	4.14	4.14	4.14	4.14
Internal Stress (*MPa*)	110	110	110	110
Change in cross-sectional area (cm^2)	24.0	24.0	24.0	24.0
Output: Derived Parameters				
	Circular Pipe		Triangular Pipe	
	FEA	Analytical	FEA	Analytical
Material cross-sectional area (cm^2)	2330.1	2522.6	10838.4	9187.8
Flow Area (cm^2)	50671.9	33544.1	14204.5	7817.7

Similar issues were found with square and elliptical pipes, as shown in Figure 7.

In the next finite element study, the material cross-section, internal pressure, and von Mises stress are fixed so that a capacitance per unit length could be calculated. Once the proper dimensions for comparing the different pipe shapes are found, as shown in Table 2 the change in volume can be calculated from the finite element model, and the fluidic capacitance per unit length can be solved. The circular cross-section, clamped or unclamped at the ends, exhibits the largest fluidic-capacitance and flow cross section. The results can be explained by the fact that circular pipes allow for the most uniform loading of the material in the wall. The material uniformly stretches up to the limiting stress, in this study half the yield strength of steel, which therefore allows for a maximum fluidic capacitance. In the other shapes studied, the stresses are non-uniform, and therefore not all of the material can be elastically loaded and stretched to achieve a high change in volume for a given fixed pressure.

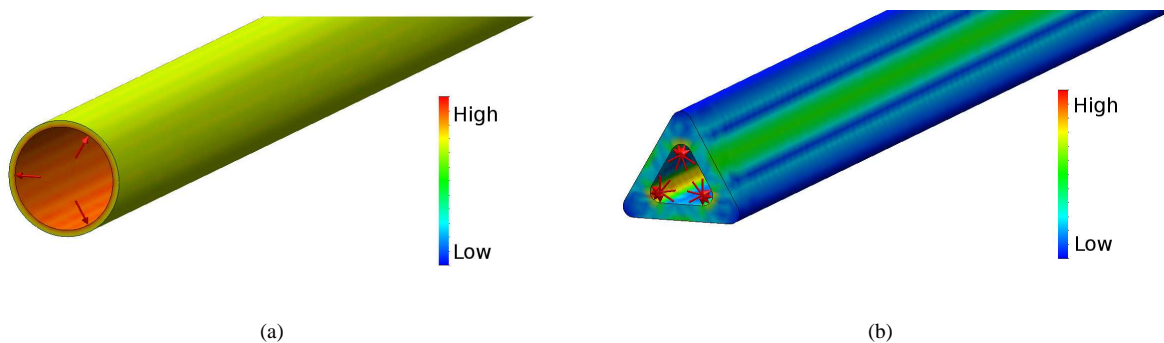(a)   (b)

Fig. 6. (a) Cylindrical pipe with uniform stress field. (b) Triangular pipe with non-uniform stress field and stress concentration at the corners on the inner side.

Given the conclusion that the greater the uniformity of stress in the pipe the greater the fluidic capacitance, another possible design is investigated involving spherical nodes attached to a pipe, as shown in Figure 8. The amount of material volume per unit fluidic capacitance of a spherical element is derived in the Appendix. A sphere requires approximately one third the amount of material required for a cylindrical pipe to achieve the same fluidic capacitance. The material per unit
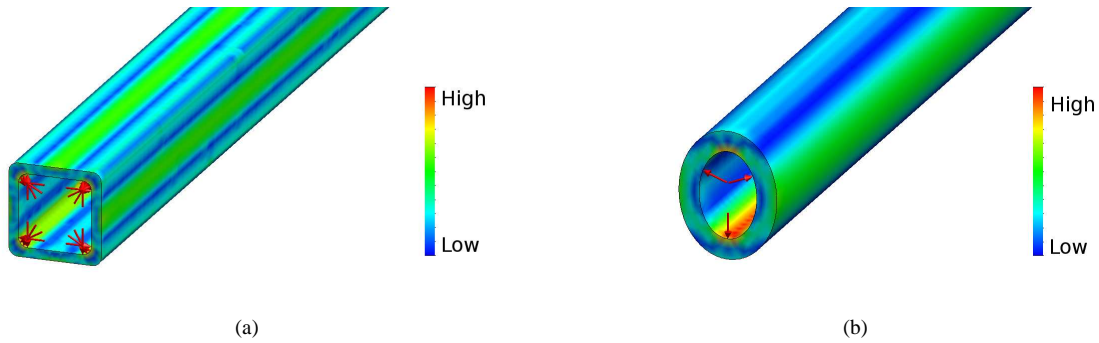
Fig. 7. (a) Square pipe with non-uniform stress field and stress concentration at the corner on the inner side. (b) Elliptical pipe with non-uniform stress field and higher stress levels on the major axis.

Table 2. Results from FEA simulations on different cross-section.

	Circular Uncapped	Circular Capped	Triangular	Square	Ellipse	Rhombus	Rectangle
Input:Independent Parameters							
Pressure (*MPa*)	11.37	11.37	11.37	11.37	11.37	11.37	11.37
Material CA (*cm²*)	20.32	20.26	20.32	20.26	20.32	20.26	20.13
Internal Stress (*MPa*)	113	110	109	118	106	115	100
Output:Derived Parameters							
△ **Area** (*cm²*)	0.077	0.090	0.006	0.013	0.013	0.006	0.006
Flow Area (*cm²*)	81.03	91.55	14.65	25.81	17.10	24.78	16.39

capacitance of a sphere is as follows.

$$m_{sphere} = \frac{PE}{\sigma_y^2(1-\nu)} \tag{5}$$

In equation 5, P is the pressure variation, E is the elastic modulus, σ_y is the yield stress and poisson's ratio. From the given analysis, spherical nodes on a pipe would yield the largest amount of fluidic capacitance for the least amount of material. For the analyses carried out here the material properties of steel have been chosen, however, in principle any other material could have been considered.

4 Lumped-Element Model of RO System

Accumulators and a pipe with spherical nodes have been found to be valid options to smooth pressure pulsations. The next step in the analysis is to calculate how much fluidic resistance is required for the given application. In order to estimate
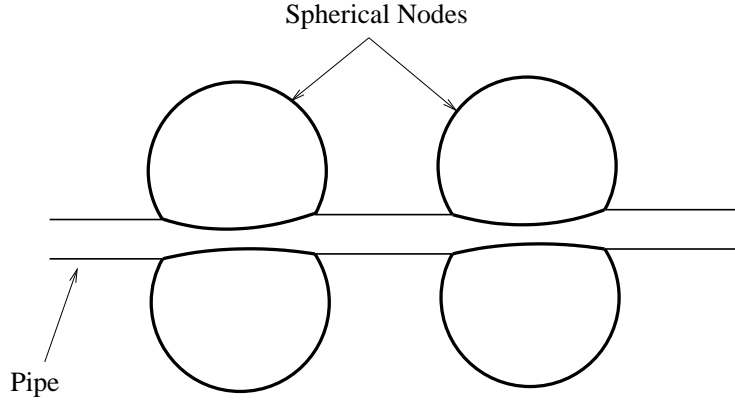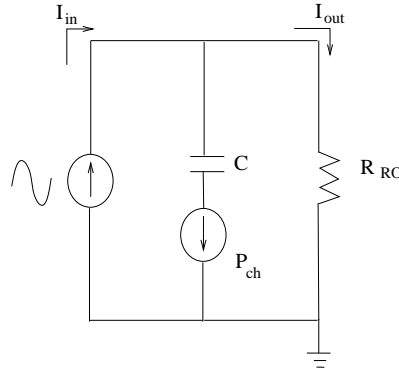
Fig. 8. Spherical capactive elements.

Fig. 9. Circuit diagram for Input-Output model. I_{in} is the incoming pulsating flow and I_{out} is the flow to the resistor. P_{ch} is the line charge pressure and is only present if an accumulator is used. R_{RP} is the resistance of the RO membrane and C is the capacitance of the fluidic capactitive element.

the necessary fluidic capacitance, the entire system is modeled using a lumped parameter model. The model includes the wave-paddle pump, pipeline, and RO membrane. It is worth mentioning that in the lumped-element model, flow rate is analogous with current and pressure is analogous with voltage in the electrical model. It is assumed that the wave-powered pump is a displacement pump and is not pressure limited. It is also assumed that by stabilizing the flow, pressure fluctuations will be reduced. The pipe connecting the wave paddle to the RO system can be modeled as an infinite chain of resistors, inductors, and capacitors that can be approximated as one equivalent link in a chain [13], as shown in Figure 9. In Figure 9, the current source represents the wave paddle, the resistor represents the RO membrane, and capacitor represents a fluidic capacitance element. Based on this circuit the transfer function is as follows.

$$\frac{I_{out}}{I_{in}} = \frac{1}{LCs^2 + (R_{pipe} + R_{RO})Cs + 1} \tag{6}$$

The variable I_{out} is the flow through the RO membrane, and I_{in} is the flow coming in from the wave-paddle pump. The manufacturers fluidic resistance of the desalination system, R_{RO}, is significantly larger than the resistance of the pipeline, R_{pipe}, and the inductance of the pipeline, L_{pipe}. Under these conditions the transfer function simplifies as follows.

$$\frac{I_{out}}{I_{in}} = \frac{1}{R_{RO}Cs + 1} \tag{7}$$

Using this equation, the capacitance required to achieve a specified reduction in pressure ripple is obtained. The percentage flow ripple is defined as 100 times I_{out}/I_{in}. Let ω rad/sec be the frequency of the incoming wave. The equation 7 can be modified as follows.

$$\%ripple = \frac{100}{\sqrt{(R_{RO}C\omega)^2 + 1}} \tag{8}$$
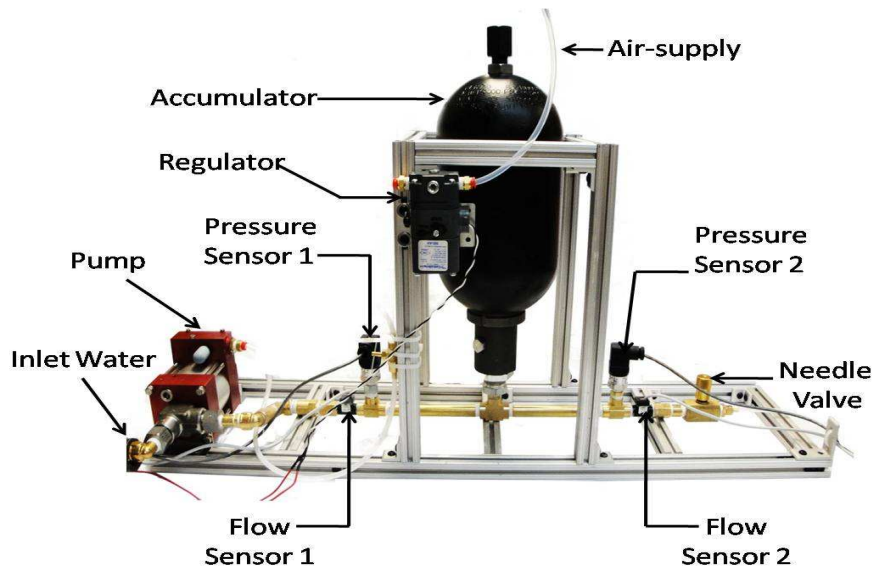
Fig. 10. Assembled experimental setup.

A smaller ripple leads to greater pressure stabilization. For this application, the desired ripple is specified and the resistance of the reverse osmosis membrane, and the average wave frequency are fixed. With these defined values, an appropriate fluidic capacitance of the system, C, can be approximated. In section 5 equation 8 is experimentally investigated. In section 6, the cost comparison of achieving desired fluidic capacitance from accumulators, elastics pipes and spheres is compared.

5   Experimental Investigation of Model

The purpose of the experiment is to identify how well the percentage ripple can be predicted when a calculated fluidic resistance is added to the system as shown in Figure 9. Figure 10 shows the experimental set up, and Figure 11 shows a flow chart of the experimental setup. While either elastic hosing or an accumulator could be used as the capacitive element in the experiment, the accumulator was selected for the experiment because of its compact nature. The cyclic pressure waves are created using a pressurized-air driven pump. An air-regulator is controlled by a LabView program to create sinusoidal pressure waves. A large water supply is connected to the pump. The Reynolds number of the fluid in experiment is matched to that of the planned scaled system. The water passes by the accumulator and exits through a needle valve. The needle valve mimics the fluidic resistance of the reverse osmosis membrane.   The resistance of the needle valve is defined as follows.

Table 3.   Description of the experimental setup as shown in Figure 10.

| Object	Function
Pressure Sensor 1	Measures the gauge-pressure at the inlet
Pressure Sensor 2	Measures the gauge-pressure after accumulator
Flow Sensor 1	Measures the flow-rate at the inlet
Flow Sensor 2	Measures the flow-rate at the outlet
Regulator	Controls the air-flow into the pump
Pump	Provides incoming pulsating-flow and is driven by air
Reservoir	Contains water
Reservoir Valve	Acts like a check-valve at the outlet of the reservoir
Accumulator	Provides fluidic-capacitance
Needle Valve 1	Acts like a regulator for inlet air that drives the water pump
Needle Valve 2	Acts as a resistance, like RO-membrane
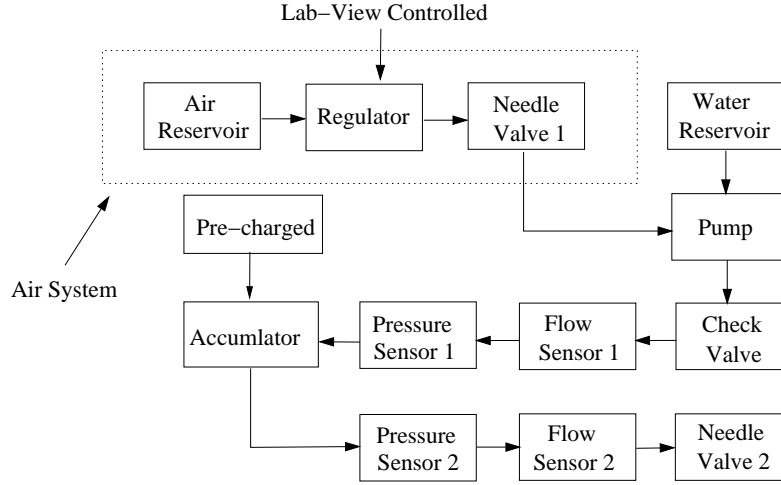
Fig. 11.   Flowchart for experimental setup.

$$R = \frac{P_{line}}{Q_{out}} \qquad (9)$$

In equation 9, P_{line} is the pressure before the needle valve and Q_{out} is the volumetric flow exiting the needle valve.

The effect of including an accumulator to the system is shown in Figure 12(a), and demonstrates that adding fluidic capacitance to the system stabilizes the flow. It should be noted that the mean pressure is substracted from the values displayed in the plot to highlight the damped pressure fluctuations. In Figure 12(b), the estimated ripple described in equation 8 is compared to the experimentally observed ripple. The ripple is plotted against the non-dimensional parameter $\alpha = RC\omega$. In the experiment the wave frequency and the resistance are independently controlled parameters. The observed results are consistently off by a factor of two from the predictions. This deviation may be explained based on the dependence of R_{RO} and C on flow frequency ω and other experimental uncertainties. The experimental results suggest that the model captures the trend for low and high α values but seems to be off by a factor of two. The model does not capture the effect that happens near $\alpha = 40$. The application at hand, however, is expected to occur at α values above $\alpha = 50$ where the proposed model appears to capture the trend. Six samples were collected for each observed α value.
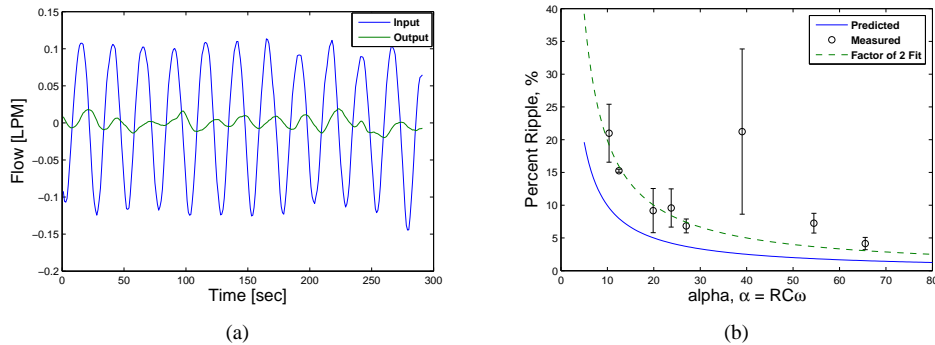

Fig. 12.   (a) Flow at the inlet and after accumulator. Average pressure substracted from presented values. (b) Comparison of % ripple based on prediction experiments. *Factor of 2 Fit* is the predicted value multiplied by a factor of 2.

6   Cost Comparison of Elastic Piping vs. Accumulator

Using equations 4 and 5 for pipes and spheres respectively, the cost of system capacitance using pipes and spheres can be estimated. The material cost is assumed to be 22 USD/kg assuming the pipes and spheres are made of steel and that material and manufacturing costs are included. Using equations 3 and 8 the required accumulator volume can be calculated
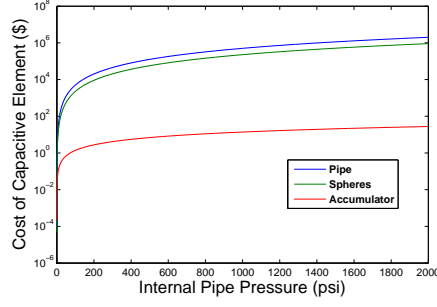
Fig. 13. Cost comparison of different shapes at varying internal pressure.
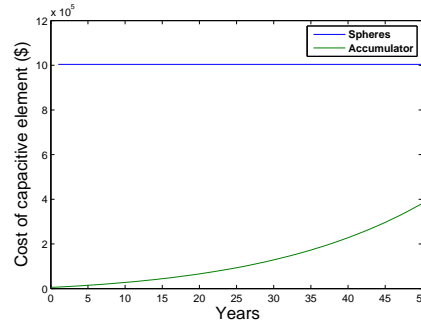

Fig. 14. Cost of ownership of Spheres and Accumulators over the course of time.

to estimate the cost of using accumulators. The precharge of the accumulator is approximated as follows.

$$P_{charge} = P_{line}(1 - \frac{\%ripple}{100})$$ (10)

Combining equations 3, 8 and 10, the equation for V_{acc} is as follows.

$$V_{acc} = \frac{P_{line}Q_{out}(\%\frac{ripple}{100} + 1)^2 * \sqrt{(\frac{100}{\%ripple})^2 - 1}}{P_{charged}\omega}$$ (11)

The purchasing cost of elastic piping, spheres, and accumulators are in Figure 13. Current prices of accumulators from different vendors are tabulated in the Appendix. The cost of the capacitive system is dependent on the pressure, assuming a constant flow, at which the system must operate. Figure 14 is the cost of ownership for the different capacitive elements. While the spherical node pipe is a one time cost, even with regular bladder replacement, the cost of accumulators is significantly lower than that of elastic piping or spherical node piping to achieve equal fluidic capacitance.

7 Conclusions
In this paper, the task of developing solutions to stabilize the fluctuating flow for the desalination application has been addressed. To achieve this task, first stub-filters were studied and found impractical. Two strategies were investigated in detail namely capacitive pipes and off-the-shelf accumulators. It was possible to obtain a desired level of fluidic-capacitance from the expansion in the pipe walls so as to accommodate the rising pressure. Analytical models and FEA simulations were carried out to predict the capacitance of the pipes with different cross-sectional areas. Pipes with circular cross-sections exhibited the highest fluidic-capacitance due to uniform stress fields in the pipe walls compared to the pipes with triangular, square, and elliptical cross sections, which showed stress-concentration at the corners. A design based on the spherical nodes serving as capacitive elements was also explored and was found to be superior compared to the cylindrical pipe design. Finally, off-the-shelf accumulators were studied for the application at hand and an experimental setup was built to verify the capacitance model. The model generally underestimates the amount of fluidic capacitance to achieve a specified ripple but demonstrates the trend of lowering ripple with increasing capacitance. Finally, a cost comparison for different

fluidic-capacitance solutions over a wide range of operating pressures was carried out, and accumulators were found to be the most cost-effective solution. It is predicted that the accumulators over fifty years of operation would cost less than half of the cost of other solutions studied.

8 Acknowledgement

References
[1] Staby, W., 2011. *Clean Power From Ocean Waves*.
[2] Prasad, B. S., 2010. "Energy efficiency, sources and sustainability". *ASME Journal of Energy Resource Technology, 132*(2), p. 020301.
[3] Fronk, B., Neal, R., and Garimella, S., 2010. "Evolution of the transition to a world driven by renewable energy". *ASME Journal of Energy Resource Technology, 132*(2), p. 021009.
[4] Tzen, E., 2009. "Wind and wave energy for reverse osmosis". In *Seawater Desalination*, G. Micale, L. Rizzuti, and A. Cipollina, eds., Green Energy and Technology. Springer Berlin Heidelberg, pp. 213–245.
[5] Magagna, D., and Muller, G., 2009. *A wave energy driven RO stand-alone desalination system: initial design and testing*.
[6] Sheng, W., and Lewis, A. "Assessment of wave energy extraction from seas: Numerical validation". *ASME Journal of Energy Resources Technology, 134*, p. 041701.
[7] Morris-Thomas, M. T., Irvin, R. J., and Thiagarajan, K. P., 2007. "An investigation into the hydrodynamic efficiency of an oscillating water column". *Journal of Offshore Mechanics and Arctic Engineering, 129*(4), pp. 273–278.
[8] Whittaker, T., Leitch, J., Long, A., and Murray, M., 1985. "The q. u. b. axisymmetric and multi-resonant wave energy converters". *Journal of Energy Resource Technology, 107*(1), pp. 74–80.
[9] "Investigation of solar desalination pond performance experimentally and mathematically". *ASME Journal of Energy Resources Technology, 134*, p. 041201.
[10] http://www.resolutemarine.com/.
[11] Viersma, T. J., 1980. *Analysis, Synthesis and Design of Hydraulic Servosystems and Pipelines*. Elsevier.
[12] Doebelin, E. O., 1972. *System Dynamics: Modeling and Response*. Charles E. Merrill Publishing Company. Columbus, Ohio.
[13] Nasser, K. M., November 2000. "Development and analysis of the lumped parameter model of a piezohydraulic actuator". Master's thesis, Virginia Polytechnic Institute and State University.
[14] Timoshenko, S., and Young, D. *Engineering Mechanics*.
[15] Crandall, S., Dahl, N., and Lardner, T., 1999. *An Introduction to the Mechanics of Solids:Second Edition with SI Units*. NY: McGraw-Hill.
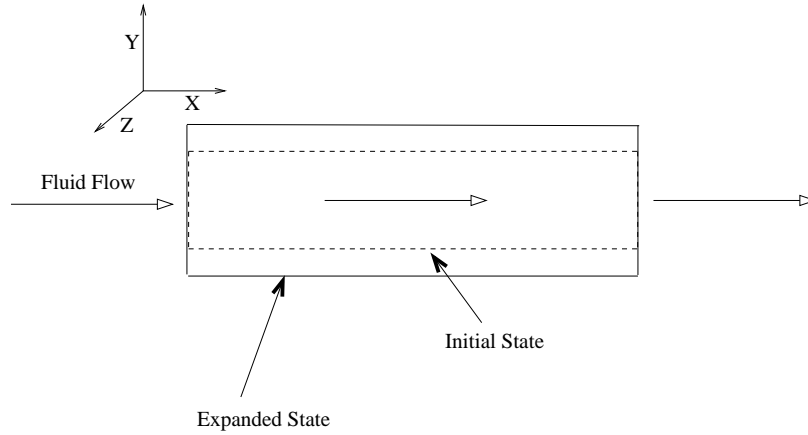
Fig. 15. Capacitance from a pipe.

9 Appendix
9.1 Fluid-Dynamics in Pipe

The inviscid Navier-Stokes equation in the X direction as shown in Figure 15 is as follows.

$$\rho\left(\frac{\partial v_x}{\partial t} + v_x\frac{\partial v_x}{\partial x}\right) = -\frac{\partial p}{\partial x} \tag{12}$$

The above equation states the pressure gradient ($\frac{\partial p}{\partial x}$) depends upon the temporal ($\frac{\partial v_x}{\partial t}$) and spatial ($\frac{\partial v_x}{\partial x}$) variations in the velocity. In other words, a variation in velocity field either space or time is likely to cause a variation in pressure along the flow direction.

In order to develop conditions in which the pressure gradient is zero i.e. pressure is uniform along the length of the pipe, a scaling analysis is carried out as follows.

$$\rho\left(\frac{v_x}{\tau} + \frac{v_x^2}{L}\right) = -\frac{\triangle p}{L} \tag{13}$$

In equation 13, the first term ($\frac{v_x}{\tau}$) represents the change of velocity with respect to time, and the second term ($\frac{v_x^2}{L}$) is the convective acceleration. The term ($\frac{\triangle p}{L}$) is the pressure loss over the length.

The velocity for an internal flow in the pipe can be estimated as follows.

$$v_x = \frac{Q}{A}$$

Here, Q is the flow rate and A is the area of cross-section of the pipe. In the current context $Q = 0.0029\ m^3$/sec and, for a circular pipe of radius $r = 0.1\ m$ i.e. area $A = 0.0314\ m^2$ yields $v_x \sim 1.0 m/sec$. The τ is 5 sec. Thus,

$$\frac{v_x}{\tau} = \frac{1.0}{5} \sim 0.2,$$

$$\frac{v_x^2}{L} \sim 0.0004$$

Both these terms are small when multiplied by the density and hence the pressure drop across the pipe is estimated to be small compared to the line pressure. Even for L of 100 meters the pressure drop $\triangle p$ is only 0.14 MPa, indicating that
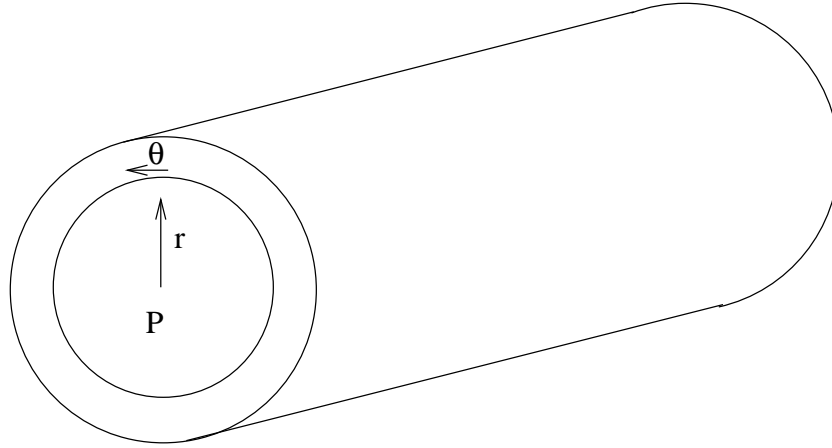
Fig. 16. Stress generation in a circular pipe under internal pressure.

the assumption of the uniform pressure is accurate. Thus, if the characteristic time scale (τ) for the variation is large and the flow rate Q or velocity v_x is small, then the pressure gradients along the pipe-length can be neglected. The central idea of extracting fluidic-capacitance from a long pipe relies upon its expansion under increasing internal pressure. In principle, any pipe with elastic properties can be applied for this purpose. Two choices to be made are (i) material selection for the pipe (Rubber, PVC, Steel, etc.) and, (ii) cross-sectional shape of the pipe i.e. circular, square, etc.

9.2   Circular Crossection

The main stress component in a cylindrical pipe is given as follows [14].

$$\sigma_{\theta\theta} = \frac{PR}{t}$$

The von-Mises stress (i.e. the equivalent stress) is given as follows.

$$\sigma_v = \frac{\sigma_y}{2}$$

We set half the yield strength as the maximum desired equivalent stress.

$$\sigma_v = \frac{\sigma_y}{2}$$

Therefore, the wall thickness 't' is as follows.

$$t = \frac{2PR}{\sigma_y}$$

The volume change is then computed as follows.

$$\varepsilon_{\theta\theta} = \frac{1}{E}(\sigma_{\theta\theta})$$

$$\triangle V_{hoop} = \triangle AL = L\pi((R+R\varepsilon_{\theta\theta})^2 - R^2) = 2L\pi\varepsilon_{\theta\theta}R^2 \rightarrow Hoop Volume change.$$

Higher order terms have been neglected.

$$\triangle V = \frac{\pi R^2 L \sigma_y}{E}$$

The amount of material for this pipe is as follows.

$$M = 2\pi R L t$$

Thus, the amount of material/capacitance for cylindrical geometry is as follows.

$$\frac{M}{\triangle V_{tot}} = \frac{4PE}{\sigma_y^2}$$

9.3 Spherical
In case of a thin-walled sphere [14], the two stress components are as follows.

$$\sigma_{\theta\theta} = \frac{PR}{2t}$$

$$\sigma_{\phi\phi} = \frac{PR}{2t}$$

Thus, in this case von-mises is as follows.

$$2\sigma_v^2 = (\sigma_{\theta\theta} - \sigma_{\phi\phi})^2 + (\sigma_{\phi\phi})^2 + (\sigma_{\theta\theta})^2$$

$$\sigma_v = \frac{PR}{2t}$$

We assume that the maximum allowable stress is equal to half the yield strength.

$$\sigma_v = \frac{\sigma_y}{2} = \frac{PR}{2t}$$

$$t = \frac{PR}{\sigma_y}$$

For finding the volume change for a closed pipe we use the following strain measures.

$$\varepsilon_{\theta\theta} = \frac{1}{E}(\sigma_{\theta\theta} - \nu\sigma_{\phi\phi})$$

$$\varepsilon_{\phi\phi} = \frac{1}{E}(\sigma_{\phi\phi} - \nu\sigma_{\theta\theta})$$

We plug in the values for both the stresses and then compute the total volume change as follows.

$$\triangle V_{total} = \frac{4}{3}\pi(R_{new}^3 - R_{old}^3) = 3R^3\varepsilon_{\theta\theta} \rightarrow Hoop volume changes$$

$$\triangle V_{sphere} = \frac{4\pi R^3(1-\nu)\sigma_y}{E}$$

Thus, the amount of material in the sphere is given as follows.

$$M = 4\pi R^2 t$$

Substituting the value of t we calculate the amount of material per unit change in the volume as follows.

$$\frac{M}{\triangle V_{tot}} = \frac{EP}{\sigma_y^2(1-\nu)}$$
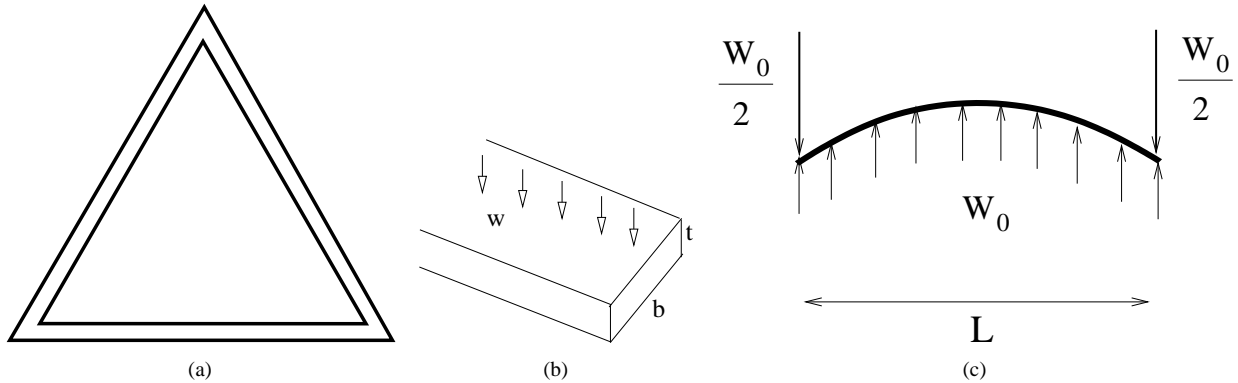
9.4 Triangular

Fig. 17. (a) Triangular cross-section (b) Uniformly Loaded beam (c) Pinned-Pinned end-conditions.

There is no analytical solution to estimate the expansion of a triangular cross-section; but we attempt this by modeling each side of the triangle as a beam with pinned-pinned end conditions and estimate the deflection of beam [15] and thereby estimate the overall change in the area. (The pinned-pinned end condition leads to an over estimate in the fluidic-capacitance of pipe). The maximum stress occurring in the pinned-pinned beam is given as follows.

$$\sigma_{max} = \frac{|M_{max}|C}{I} = \frac{wL^2}{8I}y$$

here, $M_{max} = \frac{wL^2}{8I}$, where w is the load per unit length and I is moment of inertia ($I = \frac{bt^3}{12}$). For internally loaded pressurized tubes the following equation holds.

$$\frac{w}{b} = p$$

where, p is the internal pressure. After substitution following result is achieved.

$$\sigma_{max} = \frac{3p_oL^2}{4t^2}$$

Under the pinned-pinned assumption δ (the deflection) is given as follows.

$$\delta = \frac{wx}{24EI}(l^3 - 2Lx^2 + x^3)$$

Then, total change is cross-section area per unit depth ($\triangle A = \int_0^L \delta dx$) is as follows.

$$\triangle A = \frac{p_oL^5}{10Et^3}$$

Thus, total change in cross-sectional area is given as $\triangle A_{total} = 3\triangle A = \frac{3p_oL^5}{10Et^3}$.

9.5 Accumulator Prices

Table 4. A list of commercial accumulators. Specifications taken from HYDAC (manufacturers) and Filtration Fluids (distributors).

Model Number	Pressure	Fluid Disp.	Bladder Cost	Total
	(psi)	(gallons)	(USD)	(USD)
SB330 - 6A1/112S210C	3000	1.5	276.00	905.00
SB330 - 10A1/112S210C	3000	2.5	306.00	1,194.00
SB330 - 20A1/112S210C	3000	5.0	427.00	1,521.00
SB330 - 32A1/112S210C	3000	10.0	688.00	2,250.00
SB330 - 42A1/112S210C	3000	11.0	839.00	2,339.00
SB330 - 54A1/112S210C	3000	15.0	875.00	3,163.00